Received: 10 November 2021 | Revised: 7 March 2022 | Accepted: 9 March 2022

DOI: 10.1002/mrc.5267

RESEARCH ARTICLE

WILEY

You cannot fight the pressure: Structural rearrangements of active pharmaceutical ingredients under magic angle spinning

Sebastian Scheidel | Laurina Östreicher | Isabelle Mark | Ann-Christin Pöppler

Institute of Organic Chemistry, University of Würzburg, Würzburg, Germany

Correspondence
Ann-Christin Pöppler, Institute of Organic Chemistry, University of Würzburg, Am Hubland, Würzburg 97074, Germany.
Email: ann-christin.poeppler@uni-wuerzburg.de

Funding information
German Research Foundation (DFG), Grant/Award Number: 440955393; Verband der Chemischen Industrie (VCI), Grant/Award Number: 661590; Julius-Maximilians-Universität Würzburg

Abstract

Although solid-state nuclear magnetic resonance (NMR) is a versatile analytical tool to study polymorphs and phase transitions of pharmaceutical molecules and products, this work summarizes examples of spontaneous and unexpected (and unwanted) structural rearrangements and phase transitions (amorphous-to-crystalline and crystalline-to-crystalline) under magic angle spinning (MAS) conditions, some of them clearly being due to the pressure experienced by the samples. It is widely known that such changes can often be detected by X-ray powder diffraction (XRPD); here, the capability of solid-state NMR experiments with a special focus on ^{1}H-^{13}C frequency-switched Lee–Goldburg heteronuclear correlation (FSLG HETCOR)/MAS NMR experiments to detect even subtle changes on a molecular level not observable by conventional 1D NMR experiments or XRPD is presented. Furthermore, it is shown that a polymorphic impurity combined with MAS can induce a crystalline-to-crystalline phase transition. This showcases that solid-state NMR is not always noninvasive and such changes upon MAS should be considered in particular when compounds are studied over longer time spans.

KEYWORDS

^{19}F, ^{1}H-^{13}C HETCOR, API, MAS, solid-state NMR, structural changes, XRPD

1 | INTRODUCTION

For crystalline solids, X-ray diffraction (XRD) is the state-of-the-art technique for structural investigations and structure determination. However, especially for pharmaceutical applications, an amorphous state of the active pharmaceutical ingredient (API) and/or formulation is often desired due to improved solubility and bioavailability.[1–5] Amorphous phases can be prepared by different procedures, for example, freeze drying, quench cooling, rapid evaporation of the solvent, or milling, to name only a few.[1,6] The presence of a noncrystalline solid can typically be identified by the loss of clear Bragg reflections in the X-ray powder pattern of the corresponding solid. Such a sample is referred to as "X-ray amorphous."[7–9] Due to their higher energy and lack of long-range order, such amorphous phases tend to transform into their more stable crystalline form.[3] Amorphous phases can be stabilized, for example, by poylmers, which can embed the amorphous drug in a

matrix.[10,11] Unfortunately, as the crystalline long-range order of a material disappears, most conventional structural investigation techniques, like XRD, fail to probe such a material.[1] In this case, solid-state nuclear magnetic resonance (NMR) is an excellent tool for structural investigations because NMR spectroscopy is very sensitive to the local environment and does not require long-range order.[12,13] Consequently, amorphous and crystalline solids are investigated routinely by solid-state NMR experiments for various applications, for example, for the study of phase transitions, like the single-crystal-to-single-crystal solid-state phase transition of DL-methionine[14] or the solid-state phase transitions of DL-norleucine.[15] Furthermore, even crystallization phenomena can be directly studied using solid-state NMR spectroscopy.[16,17] This has resulted in solid-state NMR being an important and versatile toolbox for the analysis of APIs and pharmaceutical products.[18,19]

However, rapid spinning under magic angle spinning (MAS) conditions leads to high pressures exercised on the sample and frictional heating, which is also increased by irradiation with long radiofrequency pulses.[20–22] Although heating of the sample can be compensated by cooling with a constant flow of temperated gas, this is not true for the pressures inside the rotor. The only method for reducing the pressure is a reduction of the spinning frequency, which leads to line broadening due to inefficient averaging of anisotropic interactions. Furthermore, spectral evaluation can become tedious if a manifold of spinning sidebands appears in the NMR spectrum recorded at slow MAS. So, increased pressures during MAS experiments cannot be easily circumvented and thus have to be kept in mind when performing solid-state NMR experiments. Pinon et al. showed that grinding and impregnation with non-solvents can also induce phase transformations of theophylline.[23] Because grinding also leads to increased local pressure on a sample, these observations demonstrate the possibility of structural changes induced by elevated pressure. In this context, we present examples of different degrees of unexpected structural changes and rearrangements, which are induced by the MAS and can be influenced by polymorphic impurities. These examples show that solid-state NMR is not always a strictly noninvasive technique to observe phase transitions in materials but can also induce and accelerate different degrees of structural changes during the measurement itself.

2 | RESULTS AND DISCUSSION

Many compounds do not alter their structure under MAS conditions. This includes typical calibration samples for MAS NMR experiments, such as L-tyrosine hydrochloride, adamantane, ammonium trifluoroacetate, or L-alanine, where phase stability during storage and MAS NMR experiments is crucial. In contrast, we observed different degrees of unexpected (structural) changes under MAS conditions for the APIs atorvastatin calcium (AVS), ezetimibe (EZI), and efavirenz (EFV) (Figure 1). AVS and EZI are used for the treatment of hypercholesterolemia,[24,25] EFV is used for the treatment of HIV.[26] The presented work is divided into amorphous (AVS and EZI), and crystalline API samples (EZI and EFV).

2.1 | Influence of MAS on amorphous samples

Overall, amorphous systems should be especially susceptible to elevated pressures or temperatures because they are thermodynamically metastable with respect to the crystalline state.[6] However, the higher aqueous solubility of amorphous samples in contrast to crystalline samples makes them attractive for pharmaceutical applications.[2,6] Because amorphous solids show no long-range order, the possibility of structural investigations by classical XRD is limited, thus making solid-state NMR spectroscopy a valuable tool for gaining structural insights.

2.1.1 | Amorphous AVS

Amorphous AVS was prepared by quench cooling. The sample was confirmed to be amorphous by X-ray powder diffraction (XRPD) measurements (Figure 2, top). Furthermore, ^{1}H NMR measurements in solution were used to rule out sample degradation (Figure S1). The obtained amorphous sample was then divided into two parts; a reference sample was stored at room temperature over silica gel at a relative humidity of 10%, while the other sample was subjected to MAS conditions at a MAS frequency of 20 kHz. The MAS sample was cooled to 273.2 K during the measurements to compensate for frictional heating and heating caused by the irradiation with long radiofrequency pulses, resulting in a calibrated sample temperature of 309 K. After 12 h of MAS, XRPD powder patterns of the MAS sample as well as the reference sample were recorded. Afterward, the MAS sample was again subjected to MAS conditions for further 12 h, and again XRPD powder patterns were measured. From this point onwards, both samples were stored at room temperature over silica gel at a relative humidity of 10%. During MAS ($t = 0$–12, $t = 12$–24 h), ^{1}H MAS, ^{1}H-^{13}C

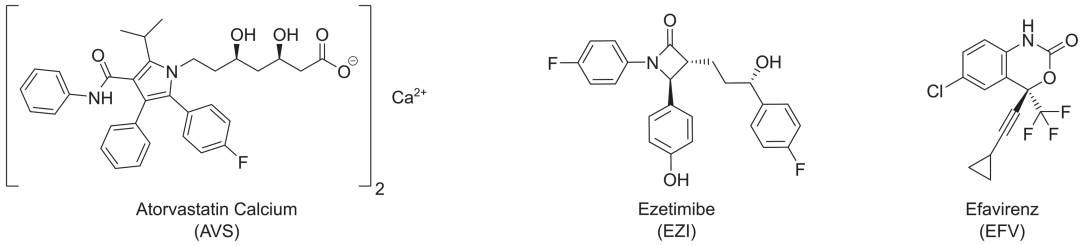

FIGURE 1 Structural formulas of the active pharmaceutical ingredients (APIs) atorvastatin calcium (AVS), ezetimibe (EZI), and efavirenz (EFV)

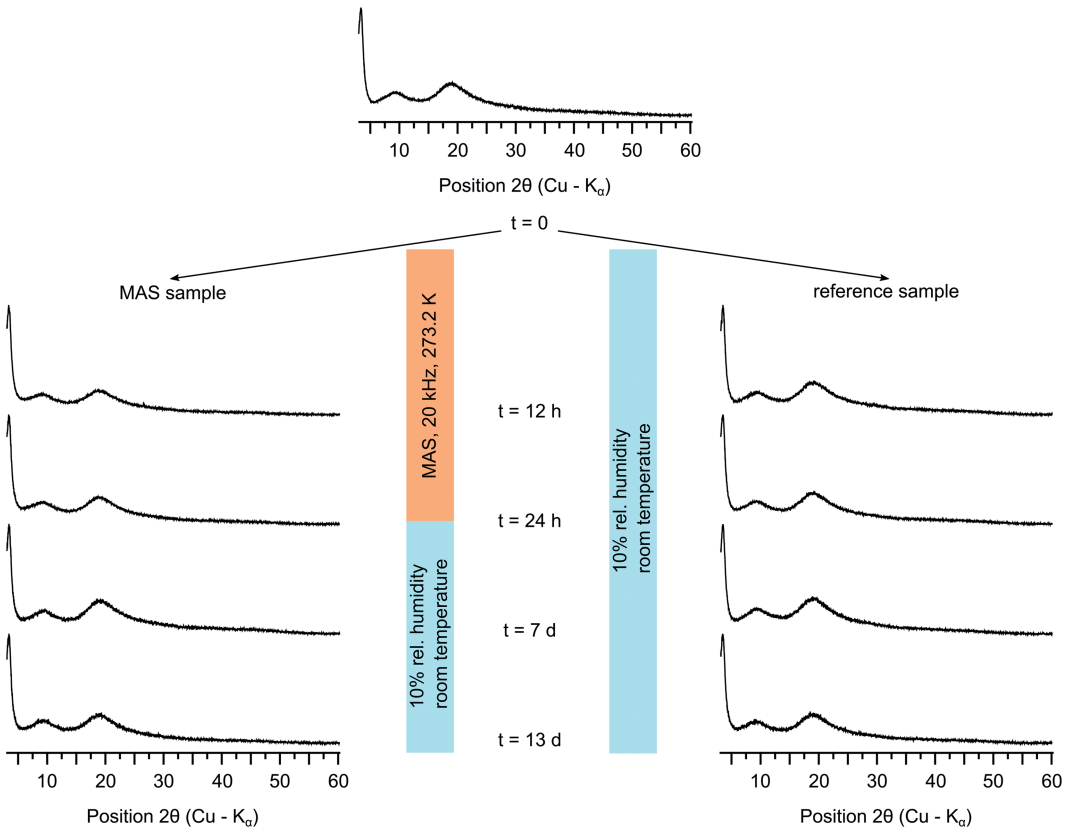

FIGURE 2 X-ray powder diffraction (XRPD) patterns monitoring amorphous atorvastatin calcium (AVS). The sample was divided into a magic angle spinning (MAS) sample and a reference sample. The reference sample was stored at room temperature and 10% relative humidity over silica gel. The MAS sample was subjected to two 12 h periods of MAS and afterwards also stored at room temperature and 10% relative humidity over silica gel

CP/MAS as well as ^{1}H-^{13}C frequency-switched Lee–Goldburg heteronuclear correlation (FSLG HETCOR)/MAS NMR experiments were recorded to monitor possible structural rearrangements.

The loss of clear Bragg reflections in the individual powder patterns (Figure 2) shows that the sample was amorphous at all times. A comparison of the ^{1}H MAS and ^{1}H-^{13}C CP/MAS NMR spectra during the two MAS periods (Figure S2) also showed that the amorphous AVS structure remained unchanged under MAS conditions.

The improved resolution in ^{1}H-^{13}C FSLG HETCOR MAS NMR experiments (Figure 3) due to the suppression of ^{1}H-^{1}H homonuclear dipolar couplings during the FSLG period, leads to much better resolved signals than in the ^{1}H 1D NMR spectra. Through the second dimension, the ^{13}C NMR chemical shifts are also appearing more separated. Because the ^{1}H NMR chemical shifts are highly sensitive to subtle changes in the local molecular environment, such experiments are useful for detecting molecular rearrangements. However, due to the scaling and referencing, which are required in the indirect

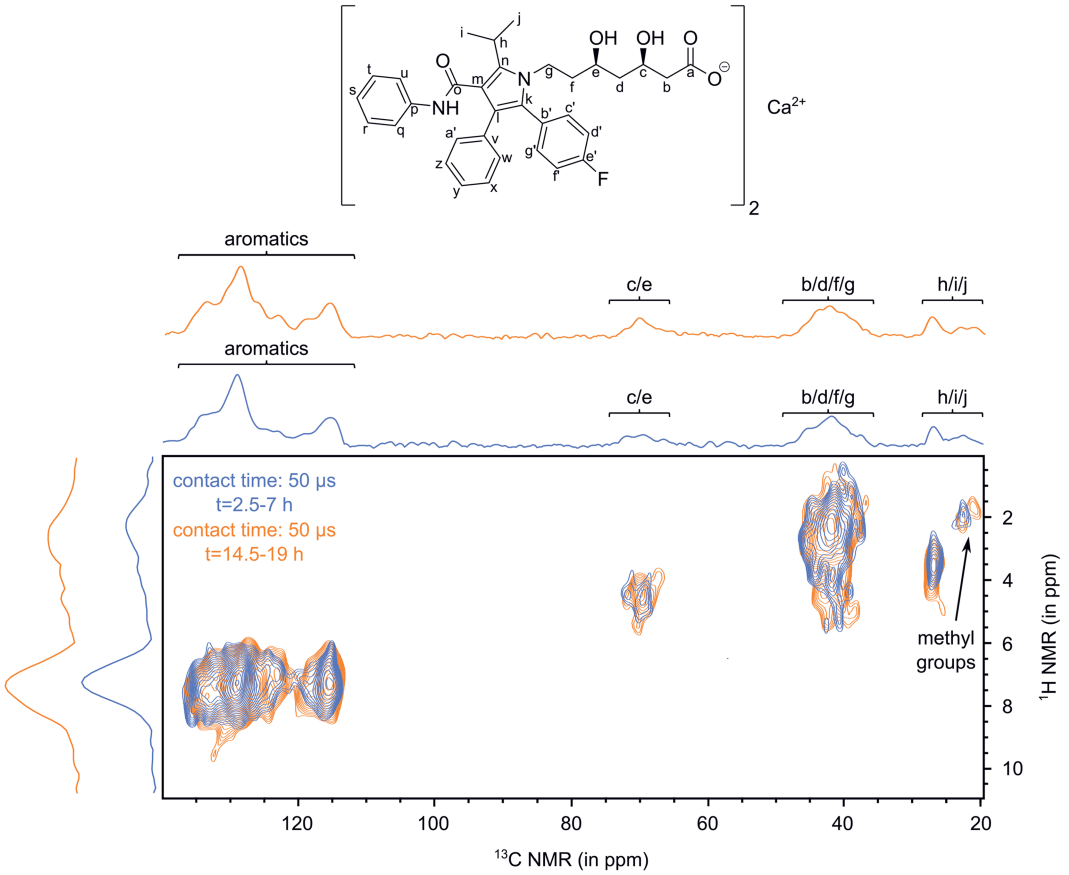

FIGURE 3 Comparison of the ^{1}H-^{13}C frequency-switched Lee–Goldburg heteronuclear correlation (FSLG HETCOR)/magic angle spinning (MAS) nuclear magnetic resonance (NMR) spectra of amorphous atorvastatin calcium (AVS) under MAS conditions for the periods $t = 0$–12 h (blue) and $t = 12$–24 h (orange). Both spectra were measured at a 600 MHz spectrometer (^{1}H: 600.4 MHz; ^{13}C: 151.0 MHz) at 273.2 K and 20 kHz MAS with a contact time of 50 µs, 80 scans, 200 increments, and a recycle delay of 1.0 s. The 1D NMR spectra are the projections of the corresponding ^{1}H-^{13}C FSLG HETCOR/MAS NMR spectrum

dimension caused by the FSLG period, small changes of the ^{1}H NMR chemical shifts in such experiments should be reviewed critically. For those measurements, short contact times of 50 µs were used, so that only contacts for directly bound CH pairs are obtained. As shown in Figure 3, the ^{1}H and ^{13}C NMR chemical shifts of the methyl groups change slightly between the two measurements. Because the changes are also evident in the ^{13}C dimension of the ^{1}H-^{13}C FLSG HETCOR NMR spectra, which is not biased by referencing or scaling, this is a clear evidence of small molecular rearrangements. That such a change is taking place for the isopropyl group can be explained by the fact that this part of the molecule is the most mobile because both the isopropyl group and the individual methyl groups can rotate. To show that such changes occur at lower sample temperatures, amorphous AVS was subjected to MAS conditions at 20 kHz and 245.0 K for 27 h, resulting in the same pressures as for the data in Figure 3, but a lower calibrated sample temperature of 287 K. A series of ^{1}H-^{13}C FLSG HETCOR NMR spectra were recorded at different time points (Figure S3). Again, a change in the resonance of the isopropyl group is observed throughout the measurements, which gets slower with time.

Therefore, although XRPD of the amorphous AVS sample showed that the long-range order is preserved upon MAS, ^{1}H-^{13}C FLSG HETCOR NMR experiments could detect small changes in the structural orientation of the isopropyl group of AVS, which was not accessible by standard 1D NMR experiments. This shows the usefulness of ^{1}H-^{13}C FLSG HETCOR/MAS NMR experiments for probing subtle structural rearrangements on a molecular level, although such experiments can be time-consuming for samples with long T1 relaxation times.

2.1.2 | Amorphous EZI

For amorphous EZI subjected to the same experimental conditions, crystallization was observed by XRPD

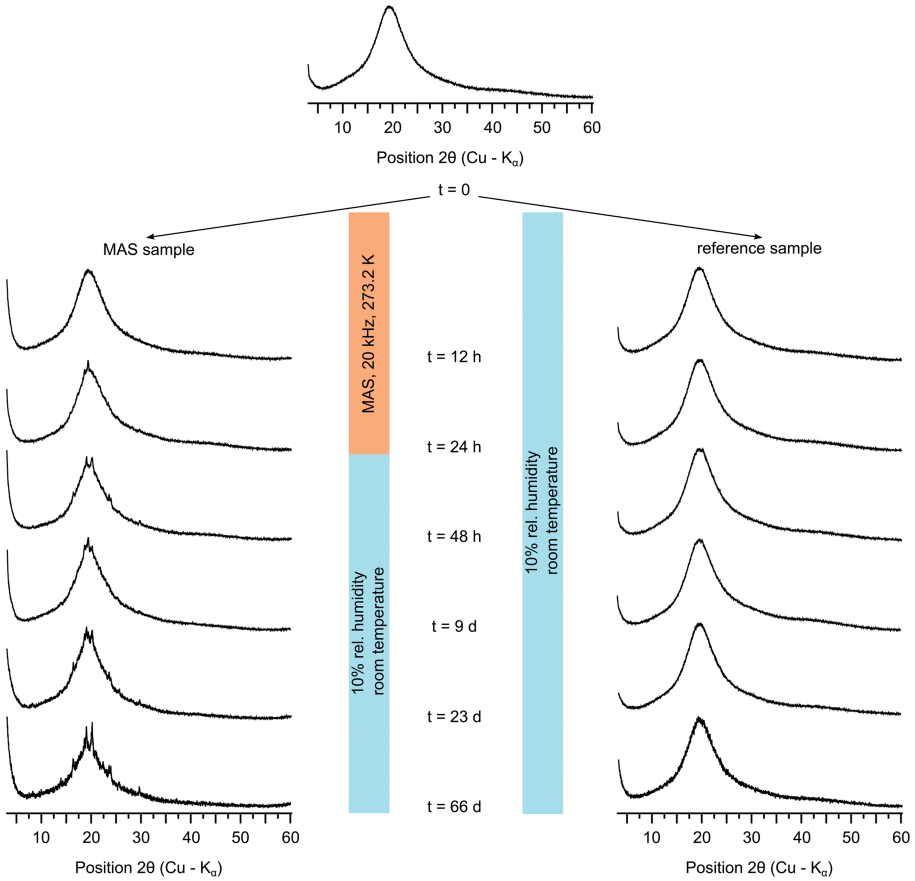

FIGURE 4 Overview of the X-ray powder diffraction (XRPD) patterns for the monitoring of the stability of amorphous ezetimibe (EZI). The initial sample was divided into a magic angle spinning (MAS) sample and a reference sample. The reference sample was stored at room temperature and 10% relative humidity over silica gel. The MAS sample was subjected to two periods of MAS conditions and afterwards also stored at room temperature and 10% relative humidity over silica gel

measurements (Figure 4). Although after 12 h of MAS ($t = 0$–12 h), the MAS sample and the reference sample were still X-ray amorphous, this is no longer the case after the second MAS period ($t = 12$–24 h), while the reference sample is still fully amorphous. The sharp signal at 18° 2θ clearly shows that amorphous EZI is transforming to a crystalline form upon MAS. Interestingly, these clear signs of crystallization are not mirrored in the ^{1}H MAS, ^{19}F MAS, and ^{1}H-^{13}C CP/MAS NMR spectra for $t = 0$–12 h and $t = 12$–24 h (Figure S5).

Again, the ^{1}H-^{13}C FSLG HETCOR NMR experiments (Figure 5) are more sensitive to rearrangements on the molecular level. Although changes in the aromatic region are difficult to observe due to severe line broadening, the aliphatic region reveals distinct changes in the ^{1}H NMR and ^{13}C NMR chemical shifts. Protons e and d of the propyl connecting fragment experience a shift to higher ppm values in the second MAS period. Although for e, two distinct carbon signals can be observed for the initial amorphous form, indicative of two predominant orientations, just one signal can be observed in the second MAS period, where the change to the crystalline phase has already begun. Knapik-Kowalczuk et al.[27] already showed by differential scanning calorimetry (DSC) that quench-cooled, amorphous EZI has a glass transition at approximately 64°C as the only thermal event, which is approximately 30 K higher than the calibrated sample temperature during MAS. To further exclude temperature as the origin of the observed changes, amorphous EZI was stored in an oven at 40°C for 48 h. Subsequent analysis by XRPD confirmed the amorphicity of the sample (Figure S6). The same sample was then subjected to 300 bar uniaxial pressure in a home-built press for 46 h. Again, the XRPD powder patterns showed no transformation (Figure S6). However, the pressure inside the rotor differs from the simple uniaxial pressure applied here. Therefore, the sample was subjected to MAS conditions for 32 h at 20 kHz and 245.0 K, which led to a change in crystallinity as observed by XRPD. Therefore, the changes in the ^{1}H-^{13}C FSLG HETCOR NMR spectra show, like the XRPD measurements, that elevated pressure under MAS can induce structural changes, in this

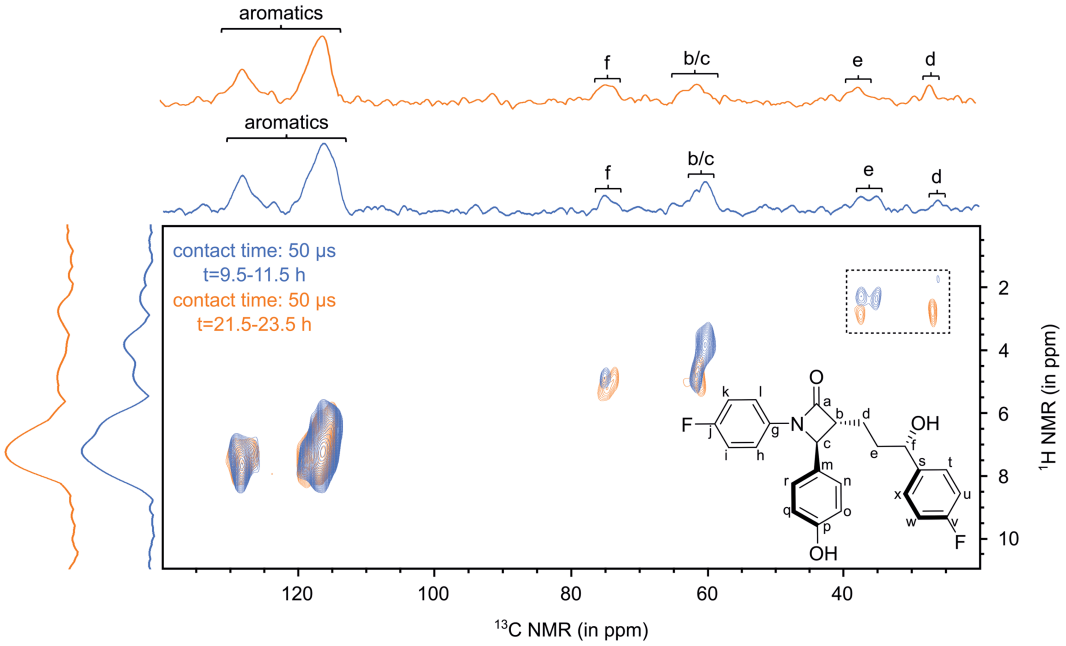

FIGURE 5 Comparison of the ^{1}H-^{13}C frequency-switched Lee–Goldburg heteronuclear correlation (FSLG HETCOR)/magic angle spinning (MAS) nuclear magnetic resonance (NMR) spectra of amorphous ezetimibe (EZI) under magic angle spinning (MAS) conditions for the periods t = 0–12 h (blue) and t = 12–24 h (orange). Both spectra were measured at a 600 MHz spectrometer (^{1}H: 600.4 MHz, ^{13}C 151.0 MHz) at 273.2 K and 20 kHz MAS with a contact time of 50 µs, 40 scans, 180 increments, and a recycle delay of 1.0 s. The 1D NMR spectra are the projections of the corresponding ^{1}H-^{13}C FSLG HETCOR/MAS NMR spectrum. The box highlights two strongly changing signals

case, the recrystallization process of metastable amorphous EZI similar to the phase transformations of theophylline[23] induced by grinding the sample.

Although the XRPD powder patterns during the two MAS periods already revealed the phase transition of amorphous EZI to its crystalline form, the consecutive XRPD measurements after storing both samples over silica gel at room temperature show that the MAS conditions have initiated the crystallization process of EZI and the MAS sample is getting more crystalline the more prolonged the sample is stored, while the reference sample still maintains its amorphous state. So the MAS conditions induced a phase transition, which continues after the end of the NMR measurements under MAS. Such a behavior can be particularly challenging if measurements of an (amorphous) sample are performed in multiple measurement blocks.

2.2 | Influence of MAS on crystalline solids

It is important to be aware that such unwanted structural rearrangements or phase transitions are not only occurring for amorphous (metastable) samples, but spontaneous (and often unwanted) structural rearrangements can also be encountered for crystalline solids.[6]

2.2.1 | Structural rearrangement of crystalline EZI

For the solid-state characterization of EZI, a variety of solid-state NMR spectra was recorded, among them a ^{1}H-^{13}C FSLG HECTOR NMR spectrum with a short contact time of 50 µs at 273.2 K. Afterwards, the sample was stored in the rotor at room temperature. After 88 days, an additional ^{1}H-^{13}C FSLG HECTOR NMR spectrum with the same resolution in the indirect dimension revealed changes in the ^{1}H NMR chemical shifts. Górniak et al.[28] and Knapik-Kowalczuk et al.[27] already showed by DSC that EZI has only one endothermic peak at 164°C,[28] which corresponds to the melting point, making changes due to elevated temperatures unlikely. A comparison of XRPD powder patterns (Figure 6) of EZI before MAS, which should represent the state of the initial ^{1}H-^{13}C FSLG HECTOR NMR spectrum, and after MAS, representing the new spectrum, showed no differences in peak positions, so no completely new phase of EZI has formed. The two ^{1}H-^{13}C FSLG HECTOR NMR spectra are shown in Figure 7, together with the assignment of the signals. Although the signals in the aliphatic region remain mostly unchanged, the larger deviations in the aromatic region, especially signals x/t and l, in the *ortho* positions of the aromatics, must be due to structural rearrangements, leading to a shielding effect of those

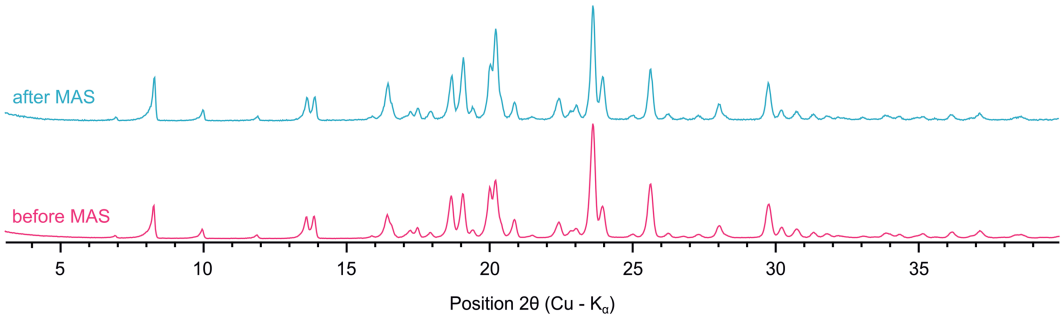

FIGURE 6 Comparison of X-ray powder diffraction (XRPD) patterns of crystalline ezetimibe (EZI) before magic angle spinning (MAS) and after MAS

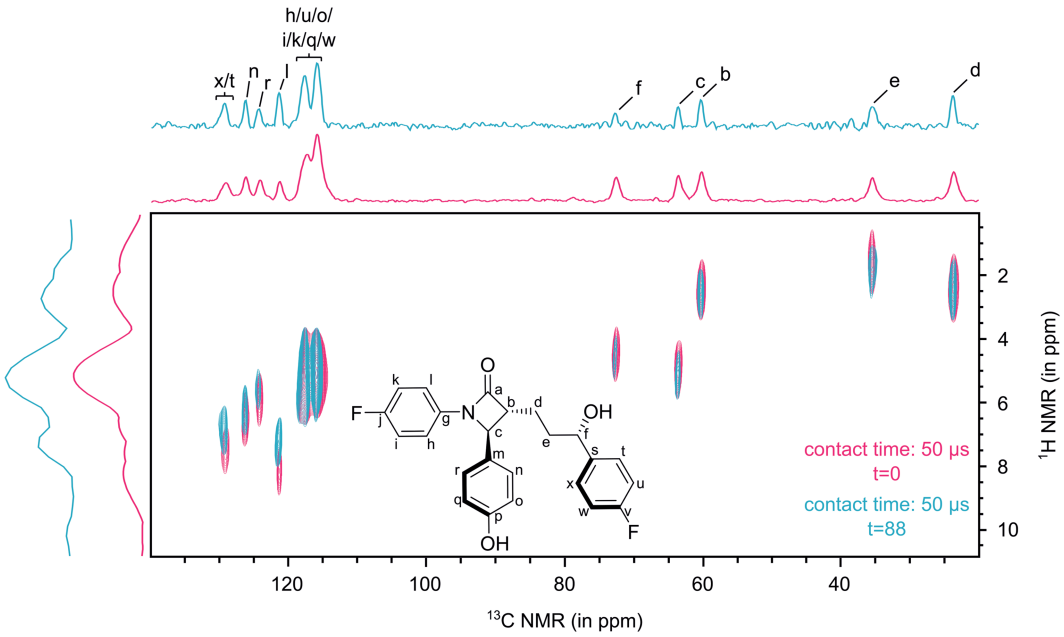

FIGURE 7 Comparison of ^{1}H-^{13}C frequency-switched Lee–Goldburg heteronuclear correlation (FSLG HECTOR)/magic angle spinning (MAS) nuclear magnetic resonance (NMR) spectra of ezetimibe (EZI). Both spectra were measured at a 600 MHz spectrometer (^{1}H: 600.4 MHz, ^{13}C 151.0 MHz) at 273.2 K with a contact time of 50 µs at a MAS frequency of 20 kHz. The ^{1}H-^{13}C FSLG HECTOR/MAS NMR spectrum at $t = 0$ (pink) was measured with 56 scans and a recycle delay of 15.0 s. The spectrum at $t = 88$ (turquoise) was recorded with 52 scans and a recycle delay of 13.0 s. Both spectra are depicted with a resolution of 120 increments in the indirect dimension. The 1D NMR spectra are the projections of the corresponding ^{1}H-^{13}C FSLG HETCOR/MAS NMR spectrum

protons. As already mentioned, small changes in the indirect dimension of ^{1}H-^{13}C FSLG HETCOR spectra are prone to errors; however, overlay of all signal areas cannot be achieved by scaling because the relative distances between the signals are different for the two spectra. Furthermore, chemical shift differences around 120 ppm in the carbon dimension, which is not influenced by scaling/processing, are a further indicator that rearrangements took place. Thus, the MAS conditions have induced a rearrangement, which continued during storage of the rotor. Zwanziger et al.[29] showed that gallium phosphide and lead nitrate single crystals subjected to external pressure show changes in chemical shifts. However, Jochum et al.[30] showed that there is no observable effect of pressure on the NMR spectrum of powdered samples because the stress cancels out for most of the sample. Nevertheless, significant stress occurs at the edges of particles.[30] This could explain why MAS induces the discussed rearrangement for EZI.

2.2.2 | Phase transition of EFV

For EFV, various polymorphs with different space groups and different numbers of molecules in the asymmetric

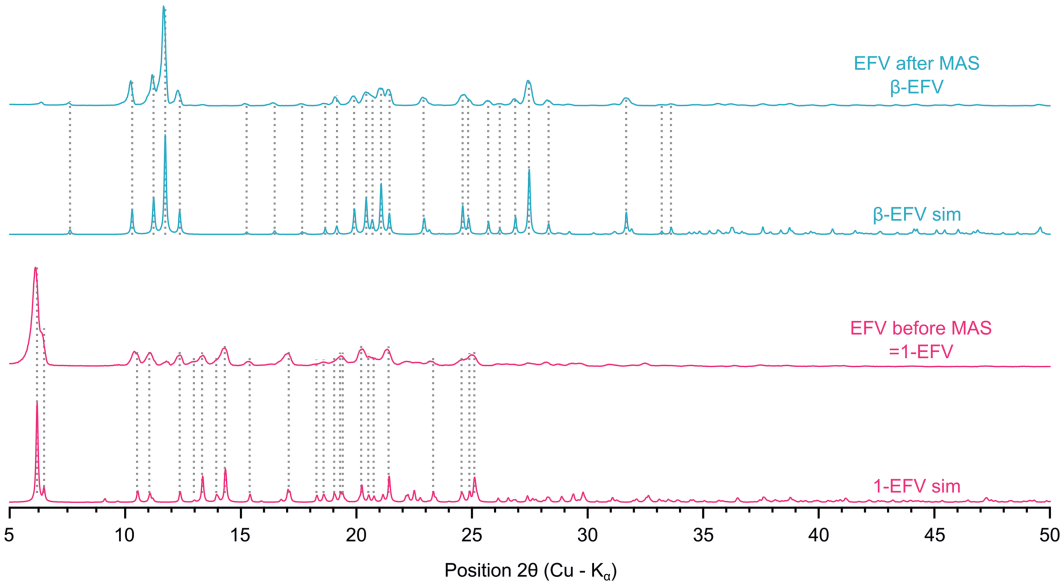

FIGURE 8 Comparison of the experimental X-ray powder diffraction (XRPD) patterns for efavirenz (EFV) before magic angle spinning (MAS) (pink) and EFV after fast MAS (turquoise) with the simulated XRPD patterns for 1-EFV (pink) and β-EFV (turquoise). The simulations were done with Mercury 3.9 (Build RC1).[33,34] For the simulations, the crystal structures of Mahapatra et al.[32] were used for 1-EFV (CSD Entry: AJEYAQ02) and by Ravikumar and Sridhar[31] for β-EFV (CSD Entry: AJEYAQ01)

unit are known, for example, β-EFV published by Ravikumar and Sridhar[31] with one molecule in the asymmetric unit or the structure published by Mahapatra et al.[32] (1-EFV) with three molecules in the asymmetric unit. The polymorph 1-EFV is the most stable polymorph at ambient conditions.[32]

The as-received sample of EFV was identified as 1-EFV (Figure 8), containing only traces of β-EFV. For the simulation employing Mercury 3.9 (Build RC1),[33,34] the crystal structure of Mahapatra et al.[32] (CSD Entry: AJEYAQ02) was used. After the solid-state NMR measurements at 263.0 K and a MAS frequency of 24 kHz, the rotor was stored for 108 days, intended to be used for further measurements. However, a comparison of a ^{19}F MAS NMR spectrum with the initially acquired data revealed significant differences between the two measurements (Figure 9). A comparison of the XRPD powder pattern of the EFV sample after MAS with the simulated XRPD powder patterns for 1-EFV and β-EFV (Ravikumar and Sridhar,[31] CSD Entry: AJEYAQ01) identified the sample as β-EFV (Figure 8). As already mentioned, 1-EFV is the thermodynamically most stable polymorph in the temperature range between 180 and 323 K. Sample temperatures were well within this range including contributions from frictional heating.[32] Furthermore, the DSC scan by Mahapatra et al.[32] shows only a single endothermic event around 140°C. The conversion is not taking place when storing the sample at ambient conditions for 3 months without MAS (Figure S7). As a further

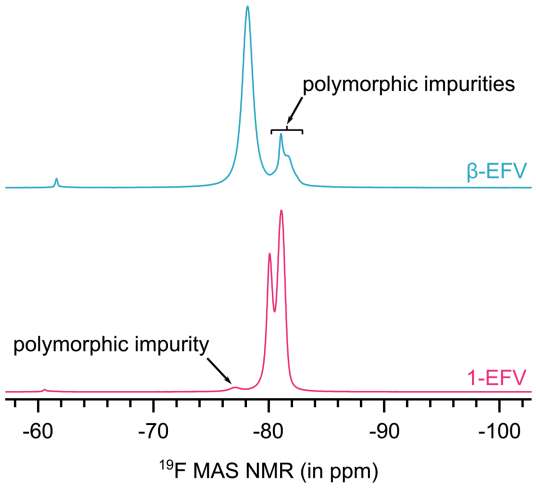

FIGURE 9 ^{19}F magic angle spinning (MAS) nuclear magnetic resonance (NMR) spectra of β-efavirenz (EFV) (turquoise) and 1-EFV (pink). Both spectra were recorded at a 600 MHz spectrometer (^{19}F: 564.9 MHz), at a MAS rate of 24 kHz at 263 K. The spectrum of β-EFV was recorded with 16 scans and a recycle delay of 5.0 s; the spectrum of 1-EFV with 64 scans and a recycle delay of 3.0 s. The peak at approximately 60 ppm corresponds to a decomposition product of EFV

control experiment, a ^{19}F MAS NMR spectrum of the 1-EFV/β-EFV mixture was recorded, the rotor then heated to 100°C for 15 h before recording another ^{19}F MAS NMR spectrum (Figure S8). Interestingly no transformation of 1-EFV to β-EFV, but the reverse conversion

of β-EFV to 1-EFV was observed. Thus, elevated temperature can be ruled out as the initiator for the 1-EFV to β-EFV phase transition. Although the original patent on EFV claimed 1-EFV to be the most stable form,[35] a detailed study of the stability of different forms including β-EFV is lacking. It is therefore possible that β-EFV is indeed more thermodynamically stable. β-EFV also has a slightly higher density than 1-EFV (approximately 0.07 $g \cdot cm^{-3}$). Thus, Le Chatelier's principle would suggest a shifting of equilibrium to the denser β-EFV if external pressure is applied. When looking at the ^{19}F MAS NMR spectra of 1-EFV, two of the three molecules in the asymmetric unit have a different environment to the third leading to two peaks in the ^{19}F NMR spectrum. For β-EFV, just one major peak can be observed, alongside another weaker signal at lower ppm values, which most likely corresponds to remaining 1-EFV. Furthermore, Ataollahi et al.[36] showed that ball-milling of 1-EFV led to the formation of amorphous EFV, which then crystallized as β-EFV consistent with the formation of β-EFV under high stress conditions. So the crystalline-to-crystalline conversion from 1-EFV to β-EFV is an example of how MAS conditions can change a samples' nature and make repeated measurements on the same sample difficult. For investigating if this phase transition is a result of contamination with traces of β-EFV, crystals of pure 1-EFV were obtained with the layering method, using acetonitrile and water (Figure S9). A ^{19}F MAS NMR spectrum was recorded using a 1.3 mm rotor and 59 kHz MAS, thus exercising an even larger pressure than for the 3.2 mm rotor, before and after storage for 7 months at room temperature (Figure 10a). No transformation of 1-EFV was observed in the absence of a polymorphic impurity.

It was shown that the crystalline-to-crystalline phase transition of EFV is only taking place if an "impurity" of the other polymorph (viz., β-EFV)—concomitant with MAS induced pressure—is present in the sample. Thus, it is of interest, if this phase transition can also happen with other impurities. The most relevant case would be the marketed formulation of EFV, because the excipients in this tablet will act as "impurity" and crystalline 1-EFV is identified by ^{19}F MAS NMR in those tablets (Figure 10b), EFV Teva 600, which is the generic medicine of ATRIPLA®. Besides 600 mg EFV, the tablet's core contains microcrystalline cellulose, hydroxypropylcellulose, sodium laurylsulfate, sodium starch glycolate (Type A), Poloxamer 407, and magnesium stearate. A ^{1}H-^{13}CP/MAS NMR spectrum of the tablet's core with assignment of the excipients is shown in Figure S10. Because none of these excipients contains fluorine, the ^{19}F MAS NMR spectra are an excellent tool for probing if EFV inside the tablet is undergoing a phase transition. Even after several NMR experiments under fast MAS conditions, storing of the rotor for 30 months and repetitive NMR experiments under fast MAS (60 kHz), the sample still exhibited its 1-EFV polymorphic form as evidenced by the ^{19}F MAS NMR spectrum (Figure 10b). Thus, it could be shown that the crystalline-to-crystalline phase transition of EFV is only taking place if β-EFV is present in the sample, but not in the presence of other excipients.

3 | EXPERIMENTAL PART

3.1 | NMR measurements

^{1}H NMR spectra in solution for ruling out sample degradation were recorded at an Avance III HD 400 (^{1}H: 400.1 MHz) spectrometer of Bruker Biospin. The chemical shifts are stated relative to the residual proton signal of the used solvent as an internal standard.

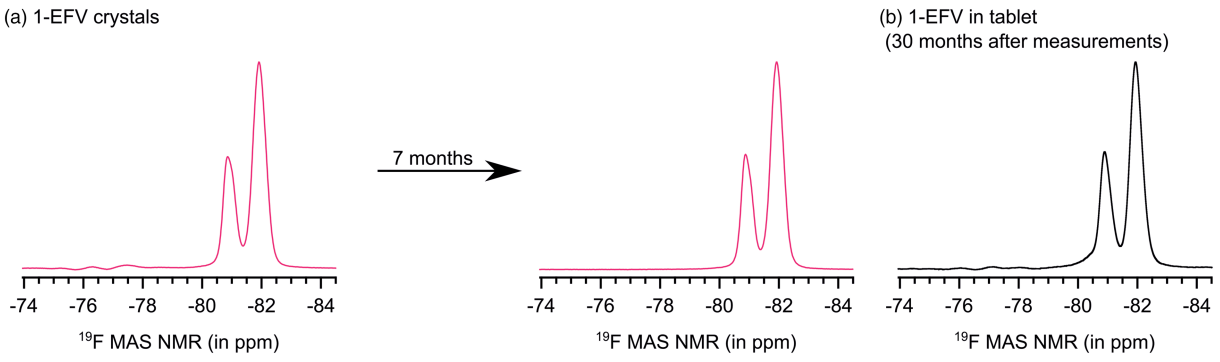

FIGURE 10 ^{19}F magic angle spinning (MAS) nuclear magnetic resonance (NMR) spectra of freshly crystallized 1-efavirenz (EFV) before and after storage for 7 months at room temperature (a) and 1-EFV in its marketed formulation EFV Teva 600 (b). All spectra were recorded at a 600 MHz spectrometer (^{19}F: 564.9 MHz), at a MAS rate of 59 kHz and 296 K with 16 scans and a recycle delay of 3.0 s. Baseline distortions between −74 ppm and −80 ppm are spectrometer artifacts

Solid-state NMR spectra were recorded at a Bruker Avance III HD 600 (^{1}H: 600.4 MHz) spectrometer using a 3.2 mm rotor for moderate MAS frequencies up to 24 kHz. The Magic Angle was set using KBr, and the frequency scale was calibrated with the carbon signal of adamantane at 38.48 ppm. With α-glycine, the 90° pulses for ^{1}H (nutation frequency 100 kHz), the power level during the CP contact pulses, and the decoupling duration were determined. For ^{19}F, ammonium trifluoroacetate was used to determine 90° pulses (nutation frequency 100 kHz). Experiments were carried out at 273.2 or 263.0 K, with the actual sample temperature being higher due to frictional heating. For measurements at 273.2 K, the calibrated sample temperature is 309 K at a MAS frequency of 20 kHz. The temperature calibration was performed using a physical blend of KBr and adamantane as described by Purusottam et al.[20] (Figure S11). For the measurements under fast MAS conditions (59 kHz,) a 1.3 mm rotor was used. The frequency scale was calibrated using the ^{1}H NMR signal at 4.90 ppm of H-β-Asp-Ala-OH. Measurements using the 1.3 mm rotor were carried out at 296.0 or 245.0 K. Samples were dried in vacuo prior to usage and MAS was done using nitrogen gas.

3.2 | XRPD measurements

XRPD powder patterns were obtained using the *Bragg–Brentano geometry* at a Bruker D8 Discover diffractometer operating at room temperature. The powders were scanned by monochromatic Cu K_α radiation at 1.5418 Å using a slit-width of 1.2 mm.

3.3 | Preparation of amorphous samples

For the preparation of amorphous samples by quench-cooling, a sample of the API was heated in a snap-cover glass until the sample was molten completely and then placed in liquid nitrogen to produce a glassy solid. The samples were then dried in vacuo and used immediately.

3.4 | Preparation of 1-EFV

For the preparation of crystals of 1-EFV, water was placed in a test tube and a small layer of acetonitrile was placed above. Afterward, a solution of EFV in acetonitrile was added. Crystals were collected after 24 h and dried in vacuo to afford 1-EFV as a white solid.

4 | CONCLUSION

For three APIs, namely, AVS, EZI, and EFV, various degrees of structural changes during MAS conditions could be observed either in their amorphous or crystalline forms. These (unwanted) structural changes include small molecular rearrangements as for amorphous AVS or crystalline EZI and complete phase transitions, as the amorphous-to-crystalline phase transition of EZI or the crystalline-to-crystalline phase transition for EFV. Although XRPD measurements were able to identify phase transitions, this was not the case for smaller structural rearrangements on a molecular level. Similarly, those subtle differences were also not captured by standard 1D solid-state NMR experiments. In these cases, ^{1}H-^{13}C FSLG HECTOR/MAS NMR spectra showed to be especially useful in monitoring a solid systems' stability due to higher resolution in the ^{1}H dimension. However, for systems with unfavorable T1 relaxation times, repeated ^{1}H-^{13}C FSLG HECTOR/MAS NMR experiments become rather time-consuming and unfeasible, possibly leaving many small structural rearrangements undetected. Structural changes described here can be attributed to the high pressure experienced by the sample under MAS conditions because the cooling of the samples counteracted temperature effects due to frictional heating. Thus, when performing solid-state NMR experiments under MAS conditions, the possibility of structural changes due to increased pressure should always be kept in mind. This holds true especially for situations, where not all necessary measurements of a sample can be performed in a sufficiently short time, and the sample has to be stored for days, weeks, or even months between measurements. Furthermore, although the pressure changes in the sample due to MAS are arguably higher than during transport, it should be kept in mind that the presence of impurities in combination with changes in pressure during transport could also initiate phase changes, which could proceed upon storage.

ACKNOWLEDGEMENTS

We gratefully acknowledge funding by the German Research Foundation (DFG) project number 440955393 and financial support from the Verband der Chemischen Industrie (VCI) in the form of a material cost. Open Access funding enabled and organized by Projekt DEAL.

PEER REVIEW

The peer review history for this article is available at https://publons.com/publon/10.1002/mrc.5267.

ORCID

Ann-Christin Pöppler https://orcid.org/0000-0002-0624-1708

REFERENCES

[1] P. Bordet, A. Bytchkov, M. Descamps, E. Dudognon, E. Elkaïm, P. Martinetto, W. Pagnoux, A. Poulain, J.-F. Willart, *Cryst. Growth Des.* **2016**, *16*, 4547.

[2] B. C. Hancock, M. Parks, *Pharm. Res.* **2000**, *17*, 397.

[3] M. Habgood, R. W. Lancaster, M. Gateshki, A. M. Kenwright, *Cryst. Growth Des.* **2013**, *13*, 1771.

[4] R. Laitinen, K. Löbmann, H. Grohganz, P. Priemel, C. J. Strachan, T. Rades, *Int. J. Pharm.* **2017**, *532*, 1.

[5] T. J. Noonan, K. Chibale, P. M. Cheuka, M. Kumar, S. A. Bourne, M. R. Caira, *Cryst. Growth Des.* **2019**, *19*, 4683.

[6] B. C. Hancock, G. Zografi, *J. Pharm. Sci.* **1997**, *86*, 1.

[7] S. Bates, G. Zografi, D. Engers, K. Morris, K. Crowley, A. Newman, *Pharm. Res.* **2006**, *23*, 2333.

[8] A. C. F. Rumondor, I. Ivanisevic, S. Bates, D. E. Alonzo, L. S. Taylor, *Pharm. Res.* **2009**, *26*, 2523.

[9] S. Tada, S. Ando, T. Asaka, Y. Daiko, S. Honda, S. Bernard, Y. Iwamoto, *Inorg. Chem. Front.* **2021**, *8*, 90.

[10] Y. Yani, P. Kanaujia, P. S. Chow, R. B. H. Tan, *Ind. Eng. Chem. Res.* **2017**, *56*, 12698.

[11] S.-S. Wang, A.-W. Xu, *Cryst. Growth des.* **2013**, *13*, 1937.

[12] T. Polenova, R. Gupta, A. Goldbourt, *Anal. Chem.* **2015**, *87*, 5458.

[13] R. F. Moran, D. M. Dawson, S. E. Ashbrook, *Int. Rev. Phys. Chem.* **2017**, *36*, 39.

[14] M. M. H. Smets, S. J. T. Brugman, E. R. H. van Eck, P. Tinnemans, H. Meekes, H. M. Cuppen, *CrystEngComm* **2016**, *18*, 9363.

[15] M. M. H. Smets, S. J. T. Brugman, E. R. H. van Eck, J. A. van den Ende, H. Meekes, H. M. Cuppen, *Cryst. Growth Des.* **2015**, *15*, 5157.

[16] C. E. Hughes, P. A. Williams, K. D. M. Harris, *Angew. Chem., Int. Ed.* **2014**, *53*, 8939.

[17] P. C. Vioglio, P. Thureau, M. Juramy, F. Ziarelli, S. Viel, P. A. Williams, C. E. Hughes, K. D. M. Harris, G. Mollica, *J. Phys. Chem. Lett.* **2019**, *10*, 1505.

[18] M. Li, W. Xu, Y. Su, *TrAC, Trends Anal. Chem.* **2021**, *135*, 116152.

[19] M. K. Dudek, S. Kaźmierski, M. J. Potrzebowski, *Annu. Rep. NMR Spectro.* **2021**, *103*, 97.

[20] R. N. Purusottam, G. Bodenhausen, P. Tekely, *J. Magn. Reson.* **2014**, *246*, 69.

[21] K. R. Thurber, R. Tycko, *J. Magn. Reson.* **2009**, *196*, 84.

[22] I. Bertini, C. Luchinat, G. Parigi, E. Ravera, B. Reif, P. Turano, *Proc. Natl. Acad. Sci. U. S. A.* **2011**, *108*, 10396.

[23] A. C. Pinon, A. J. Rossini, C. M. Widdifield, D. Gajan, L. Emsley, *Mol. Pharmaceutics* **2015**, *12*, 4146.

[24] P. H. Chong, J. D. Seeger, *Pharmacotherapy* **1997**, *17*, 1157.

[25] D. Lüdeker, G. Brunklaus, *Solid State Nucl. Magn. Reson.* **2015**, *65*, 29.

[26] F. Maggiolo, *J. Antimicrob. Chemother.* **2009**, *64*, 910.

[27] J. Knapik-Kowalczuk, K. Chmiel, K. Jurkiewicz, N. T. Correia, W. Sawicki, M. Paluch, *Pharmaceuticals* **2019**, *12*, 40.

[28] A. Górniak, H. Czapor-Irzabek, A. Złocińska, B. Karolewicz, *J. Therm. Anal. Calorim.* **2021**, *144*, 1219.

[29] J. W. Zwanziger, U. Werner-Zwanziger, J. L. Shaw, C. So, *Solid State Nucl. Magn. Reson.* **2006**, *29*, 113.

[30] M. Jochum, U. Werner-Zwanziger, J. W. Zwanziger, *J. Chem. Phys.* **2008**, *128*, 052304.

[31] K. Ravikumar, B. Sridhar, *Mol. Cryst. Liq. Cryst.* **2009**, *515*, 190.

[32] S. Mahapatra, T. S. Thakur, S. Joseph, S. Varughese, G. R. Desiraju, *Cryst. Growth Des.* **2010**, *10*, 3191.

[33] C. F. Macrae, I. J. Bruno, J. A. Chisholm, P. R. Edgington, P. McCabe, E. Pidcock, L. Rodriguez-Monge, R. Taylor, J. van de Streek, P. A. Wood, *J. Appl. Crystallogr.* **2008**, *41*, 466.

[34] C. F. Macrae, P. R. Edgington, P. McCabe, E. Pidcock, G. P. Shields, R. Taylor, M. Towler, J. van de Streek, *J. Appl. Crystallogr.* **2006**, *39*, 453.

[35] L. A. Radesca, M. B. Maurin, S. R. Rabel, J. R. Moore, WO9964405, **1999**.

[36] N. Ataollahi, M. Broseghini, F. F. Ferreira, A. Susana, M. Pizzato, P. Scardi, *ACS Omega* **2021**, *6*, 12647.

SUPPORTING INFORMATION

Additional supporting information may be found in the online version of the article at the publisher's website.

How to cite this article: S. Scheidel, L. Östreicher, I. Mark, A.-C. Pöppler, *Magn Reson Chem* **2022**, *60*(6), 572. https://doi.org/10.1002/mrc.5267